METALLURGY

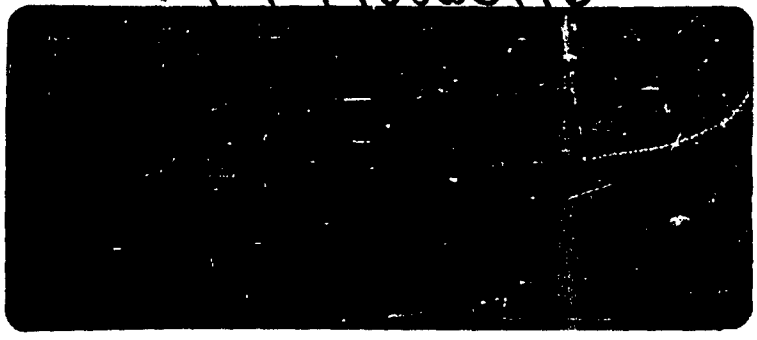

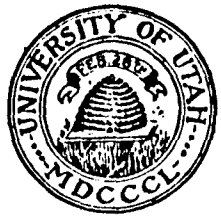

DEPARTMENT OF METALLURGY
Institute of Metals and Explosives Research

UNIVERSITY OF UTAH
SALT LAKE CITY, UTAH

NOTICE: When government or other drawings, specifications or other data are used for any purpose other than in connection with a definitely related government procurement operation, the U. S. Government thereby incurs no responsibility, nor any obligation whatsoever; and the fact that the Government may have formulated, furnished, or in any way supplied the said drawings, specifications, or other data is not to be regarded by implication or otherwise as in any manner licensing the holder or any other person or corporation, or conveying any rights or permission to manufacture, use or sell any patented invention that may in any way be related thereto.

IONIZATION WAVES FROM FREE SURFACES OF DETONATING EXPLOSIVES

A. Bauer, M.A. Cook and L.A. Rogers

September 7, 1961
AFOSR - 1335
Contract Number AF-18(603)-100
File Number 11-17-W

Project Director: M.A. Cook

Physics Division, Air Force Office of Scientific Research, ARDC, Washington 25 D.C.

WSS/CI Paper 61-20
September 1961

IONIZATION WAVES FROM FREE SURFACES OF DETONATING EXPLOSIVES

Alan Bauer, Melvin A. Cook, and Leo A. Rogers

Institute of Metals and Explosives Research, University of Utah, Salt Lake City, Utah

Western States Section, The Combustion Institute, 1961 Fall Meeting

IONIZATION WAVES FROM FREE SURFACES OF DETONATING EXPLOSIVES

A. Bauer, M. A. Cook, and L. A. Rogers

ABSTRACT

Ionization waves ejected from the free surface of condensed high explosives in various gaseous media at ambient (about 645 mm) and 0.5 mm Hg pressures are described. Framing camera and streak camera photographs correlated with electrical conduction measurements showed that a highly ionized, either highly luminous or completely transparent, precursor wave led both the shock wave and the main products of detonation propagated from the free surface. At 0.5 mm Hg this wave was transparent and non-luminous, but it always produced a burst of luminosity upon collision with the end plate of the vacuum chamber several microseconds before the opaque detonation products impacted the end plate. Measured ionization wave pressures were compared with computed ones for shock waves moving at the same velocity in the same gas. The measured pressures were in general several times greater then the pressures computed by shock wave theory for the observed velocity and initial pressure and up to 20 times greater than for the shock computed by the impedance mismatch equation. The waves from the explosive free surface appear to be highly ionized material radiated from the free surface of the explosive as a precursor wave similar, for example, to the (electron) precursor waves observed by Weyman and by Gloersen in shock tubes.

Introduction

When a condensed high explosive is detonated an ionization wave is ejected from its free surface into the surrounding gaseous medium.[1-5] This ionization wave may be luminous, transparent, or dark and opaque depending upon the gas medium and the pressure. While this school has maintained that this ionization wave is a dilute plasma moving in front of the shock wave, others[6,7] have regarded it simply as the shock wave itself in which ionization occurs in a normal and predictable manner by thermal ionization. This article presents additional evidence[4,5] that this ionized wave is actually separated from the slower moving shock wave and contains free electrons at concentrations frequently quite different than in normal thermal ionization in shock waves. Data obtained from streak camera and color framing camera sequences correlated with electrical conduction measurements for shots in various gaseous media at ambient (about 645 mm) and at 0.5 mm Hg pressure are used to distinguish these waves as well as measured pressures compared with hydrodynamically computed pressures for shocks in the medium in question traveling at the same velocities as the observed ionization waves. Comparison of the observed velocities with velocities computed for shock waves transmitted from free surfaces are also described in support of the precursor ionization wave concept.

Experimental Methods

For correlation studies a streak camera and framing camera were in some cases operated synchronously in order to obtain both recordings of the same event. Such simultaneous streak and framing photographs provide valuable, if not indispensable information for interpretation of detonation phenomena at free surfaces.

Pressure measurements were made by the "aquarium" technique[8,9] by impacting the wave in question into a transparent medium and observing the initial shock wave velocity in the transparent medium. Pressures were obtained from pressure vs velocity calibration curves from which the pressure

in the transparent medium was then related to that in the wave by the "impedance mismatch" equation[10]

$$P_i = P_w - \frac{\rho_i V_i + \rho_w V_w}{2\rho_w V_w} \qquad (1)$$

Here P_i = pressure of wave, P_w = pressure of shock wave in water (or plexiglas), ρ_i = density of the gaseous media, V_i = velocity of wave, ρ_w = density of water, and V_w = velocity of shock wave in water at impact surface. The values of V_i and V_w were obtained with the streak camera. For study of various gaseous media at 645 mm Hg pressure glass aquaria 6" X 6" X 12" were used. The explosive was mounted inside the aquarium, covered and thoroughly flushed with the desired gas before and during the shot. For pressure measurements water was poured into the aquarium to a depth of several inches and the wave impacted into it after traveling through the gas in question.

When bare explosives were fired near the water surface it was impossible to separate the ionization wave from the normal detonation shock wave owing to insufficient resolution. To overcome this the assembly shown in Fig. 1 was used. The ionization wave ejected from the explosive and moving ahead of the normal shock wave was compressed as it was "extruded" up the narrowing flask and into the relatively small diameter tubing.[5] The compressed ionization wave was then impacted into the water (or plexiglas) for pressure measurements before the much more intense blast wave from the main charge impacted a short time later to transmit an over-powering shock into the gage medium. Fig. 2 shows framing camera sequences of an ionization wave being extruded into the tube and the shock generated in the water by the extruded ionization wave.

For the studies at 0.5 mm Hg pressure the method shown in Fig. 3 was used. The system was thoroughly flushed with the desired gas, sealed and evacuated to 0.5 mm Hg as measured with a Stokes McLeod gage. The gases used in these studies were commercial products.

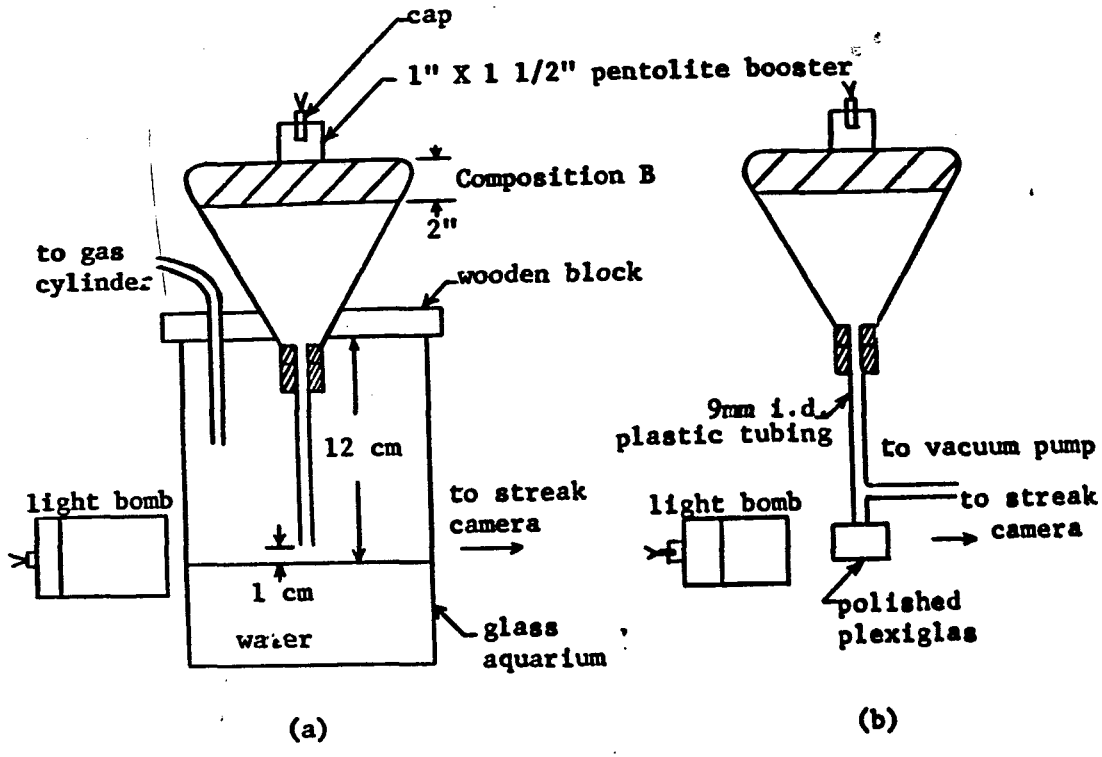

Fig. 1 Assembly used to study characteristics of compressed plasmas.

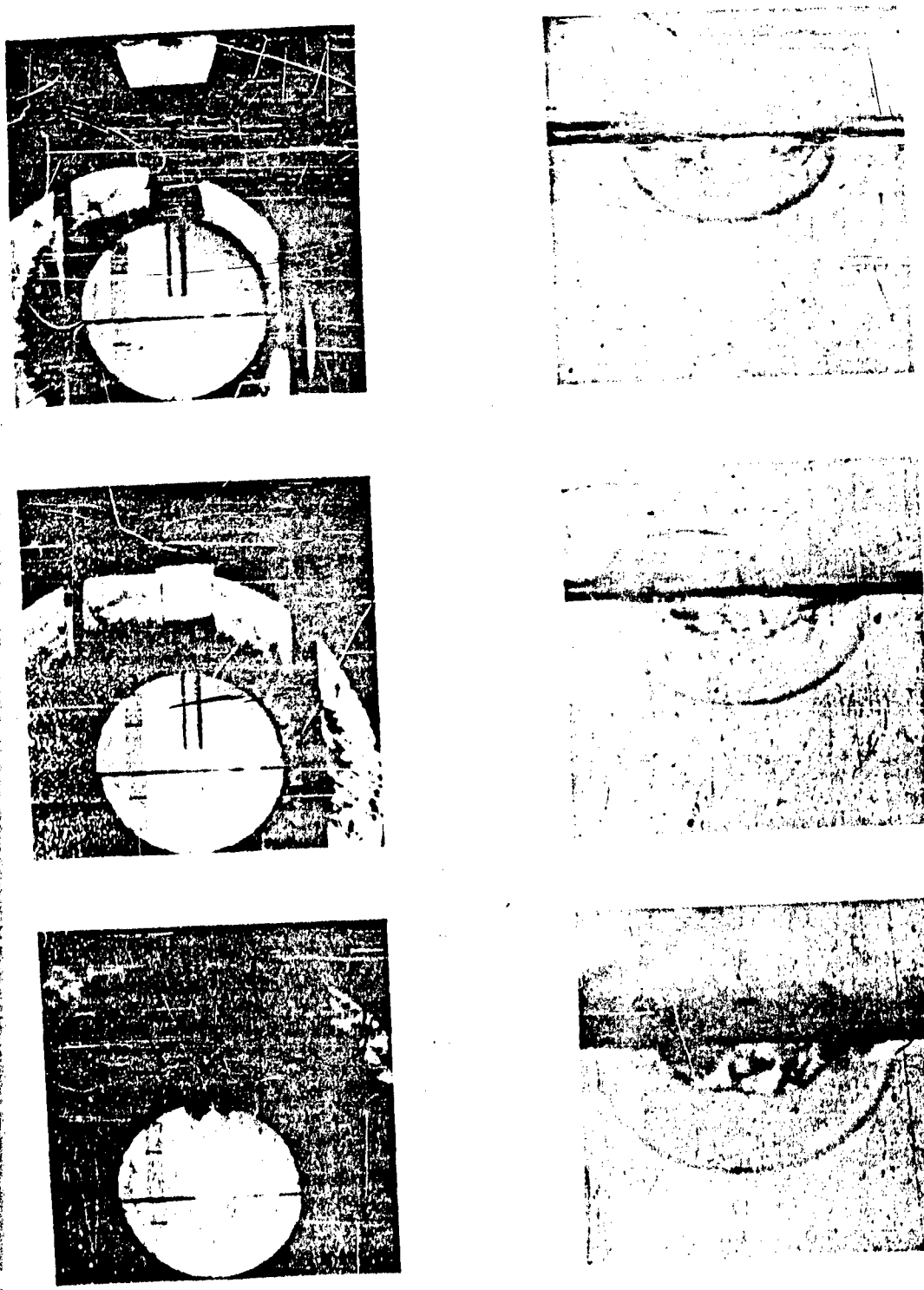

a. wave being compressed

b. shock generated in water

Fig. 2. Ionization waves extruded into glass tube and impacted into acquarium water.

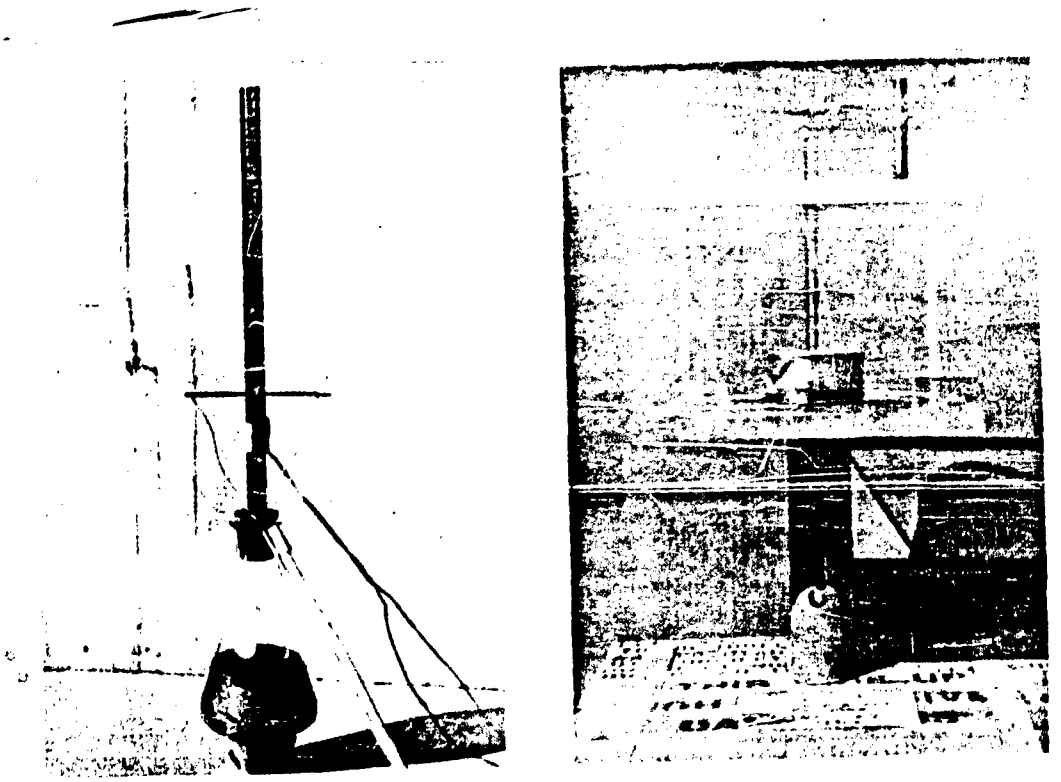

(a) (b)

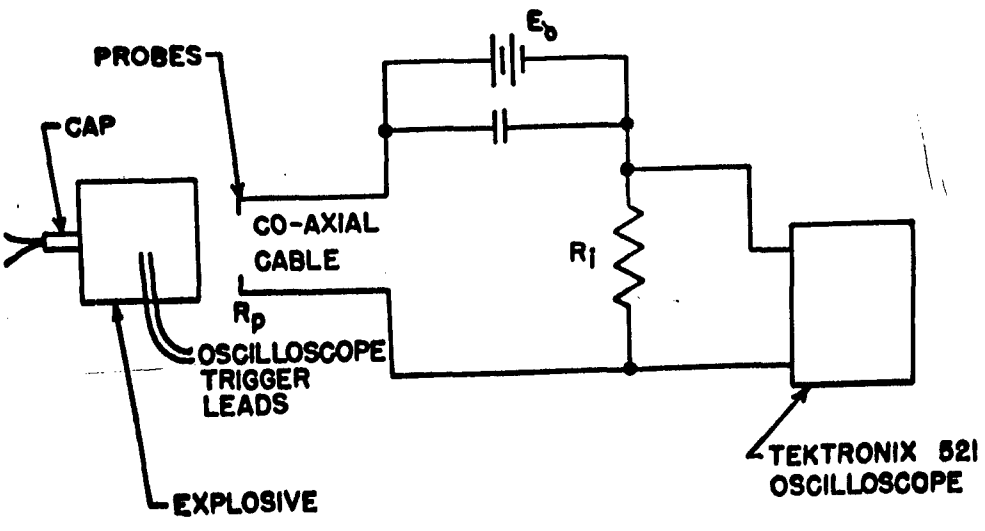

(c)

Fig. 3. Assembly used for electrical conductivity measurements.

Electrical conductivity measurements were made with the method seen in Fig. 3c the constant voltage E_o (Fig. 3c) was divided between the known internal resistance (R_i) and the unknown resistance (R_p) offered by the ionization wave as it passed into the region between the probes. By measuring the voltage drop across R_i the value of R_p was found. The conductivity of the ionization wave was determined by applying a calibration probe factor. ($\sigma = K/R_p$, where σ = conductivity, K = probe factor). The probe factor K was determined by inserting into the plastic tube a small length of pipe of the same inside diameter as the plastic tube and with a wire at its axis. With this known concentric geometry the conductivity σ was calculated from the equation [4]

$$\sigma = \frac{K}{R_p} = \frac{1}{R_p}\left[\frac{\ln b/a}{2\pi l}\right] \qquad (2)$$

where b = inside radius of cylinder. a = radius of inside wire. l = length of cylinder. Table IV lists the experimental data and probe factor.

Shock waves transmitted from the high explosive through thin inert plates were observed by the streak camera by means of back lighting with a parallel light source.

Experimental Results

Luminosity

Qualitative luminosity results are given in Table I and a few frames from several typical framing camera sequences are shown in Fig. 4. Ionization wave velocity data are given in Table II. Note that the velocity of the ionization waves decreased with increasing gas density. An important factor other than the density of medium influending velocity of the ionization waves is the ionization intensity which is determined by the chemical nature, density, diameter and length of the explosive as illustrated in Fig. 5. Because of the many variables involved, no extensive analyses of ionization wave attenuation and life-time were made in this study, these factors having been discussed previously.[1,4]

Table I: Qualitative comparisons of visible light intensity for ionization waves propagated through various gases at ambient pressures.

Explosive	Gaseous atmosphere	Ionization potential (e.v.)	Visible luminosity
D-13*	Argon	15.7	Extremely brilliant
D-13	Air	--	Bright
	Nitrogen	15.5	Bright
	Oxygen	12.5	Bright
	Carbon monoxide	14.1	Bright
	Carbon dioxide	14.5	Bright
D-13	Ammonia	11.2	Moderately bright
	Chlorine	13.2	Moderately bright
D-13	Propane	--	Non luminous-dark cloud forms
D-13	Helium	24.5	No detectable luminosity transparent cloud only
	Hydrogen	15.6	Same as in He
Composition B and tetryl	Helium	24.5	Weak momentary light at charge surface. No luminosity at long distances from charge
Composition B	Air Vacuum	--	Very low to no luminosity depending on actual pressure

* D-13 = 63/24/13 HNO_3/nitrobenzene/water

Table II: Ionization wave velocities in various gases at ambient pressure

Explosive	Gas	Velocity (m/sec) of Ionization Waves
Comp. B*	Air	8320
	Argon	8570
	Helium	8670
	Hydrogen	10400
	Air at 0.5 mm Hg	14000
D-13**	Propane	5400
	Carbon dioxide	5450
	Acetylene	6100
	Argon	6600
	Nitrogen	6700
	Carbon monoxide	7200
	Helium	7400
	Hydrogen	8150
Comp B**	Propane	6650
	Helium	8150
PETN**	Helium	7300

* Velocity 2 cm away from charge as measured with streak camera

** Approximate velocity determined from framing camera sequence averaged over 8 to 12 frames while ionization wave traveled to about 15 cm from charge surface.

a. wave from D-13 into oxygen

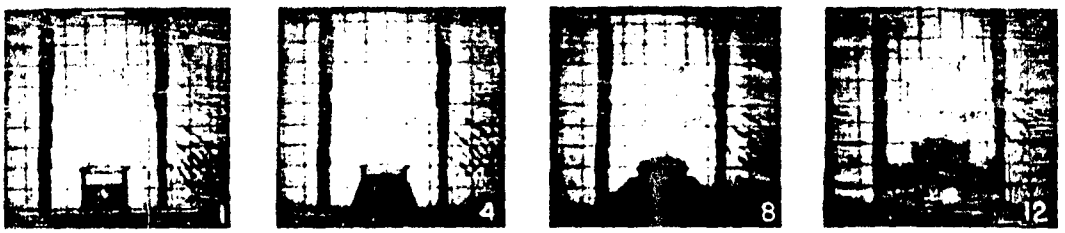

b. wave from D-13 into hydrogen

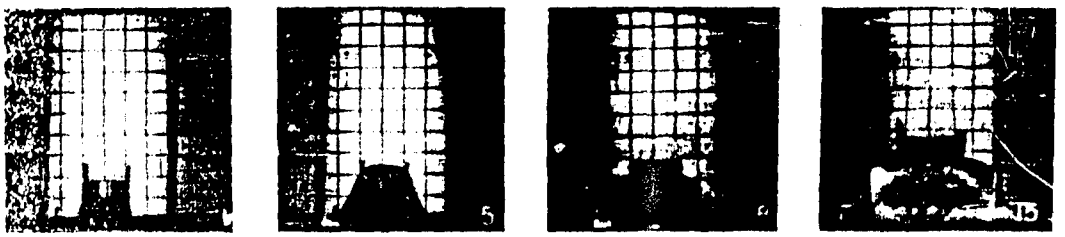

c. wave from D-13 into helium

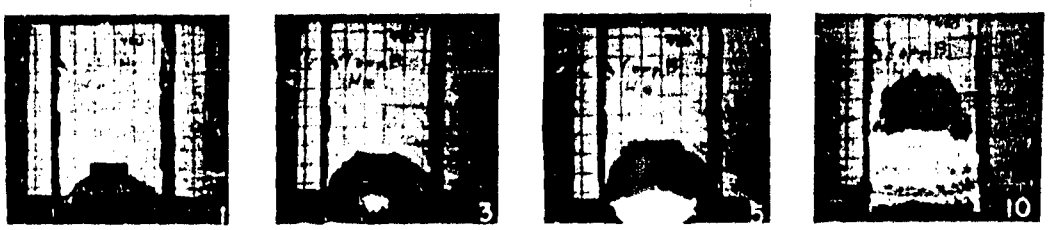

d. wave from Comp. B into helium

Fig. 4. Selected framing camera photographs of ionization waves ejected from explosive free surfaces into various gaseous media. Frame numbers shown. (1.39 μsec/frame)

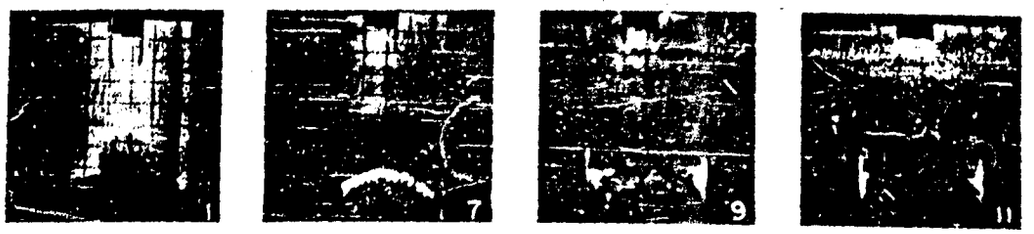

e. high voltage discharge (approx. 20 K.V.) across wave from D-13 into helium

f. burst of luminosity generated when transparent wave from D-13 traveling in helium impacted end of chamber.

g. wave from D-13 traveling first in helium and then in air. Thin polyethylene separates gases.

Fig. 4. Selected framing camera photographs of ionization waves ejected from explosive free surfaces into various gaseous media. Frame numbers shown. (1.39 μsec/frame)

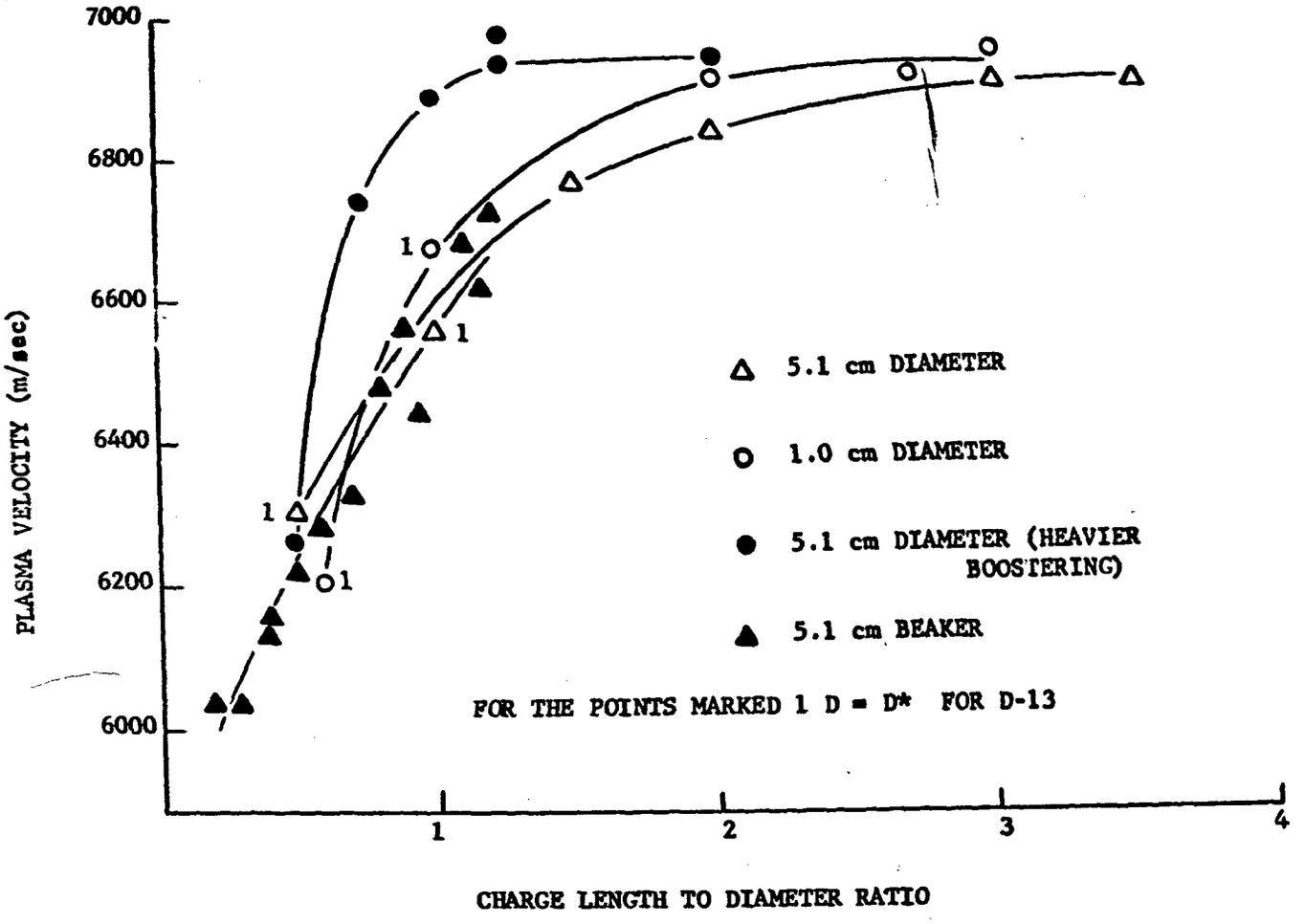

Fig. 5 Initial plasma velocity vs length to diameter ratio for 5.1 cm and 1.0 cm D-13.

Ionization and Shock Wave Pressures

Results of measurement of the ionization wave pressures are given in Table III along with corresponding values calculated from shock wave theory. Figs. 6 and 7 show graphically the results of pressure and velocity measurements as a function of gas density.

Conductivity

Estimates were also made of the rate of decay of conduction of the ionization waves as they propagated away from the free surface of the charge in various gaseous media. Figs. 8 and 9 show plots of the conduction as a function of time using bare parallel probes. In these tests the ends of the probes were cast into 1-1/2 " X 1-1/2" pentolite charges with about 20 cm of gaseous medium above the charge. The probes were placed 5 mm apart. This afforded a uniform conductivity inside the pentolite as a reference to the (integrated) conduction in the freely expanding ionization wave. The "base line" as seen in Fig. 8 was obtained by insulating the probes down to the surface of the explosive, the surface being coated with grease. Thus, the base line defined the internal explosive conduction zone so that conduction above this line was related to the intensity of the ionization wave, and the density and composition of the gaseous medium.

In order to obtain maximum conduction as a function of distance from the charge rather than integrated values, point probes (0.5 cm gap) were mounted perpendicular to the charge axis at various distances from the charge. This method also employed 1-1/2" X 1-1/2" pentolite charges and free expansion of the ionization waves. The curves all extrapolated to a common point at the charge surface. Conduction data for compressed ionization waves as measured by the method in Fig. 3a are given in Table IV. The 1/16" D probes in this case extending inside the 9 mm I.D. plastic tube were about 5 mm apart. The shapes of the oscilloscope traces shown in Fig. 10 are characteristics of the gases used (allowing for statistical fluctuations).

Table III:

Experimental and computed pressures (assumed shock) in various gases (Composition B charge)

Gas	L_i	N	V_i	M	p_w	p_i	p_s	p_i/p_s
1. Air	0.001	3	17.0 ± 0.1	51.3	Below experimental limit			
2. H_2 (0.5 mm Hg)	0.075	3	16.8 ± 0.2	50.6	1.4 ± 0.2	0.70 ± 0.10	0.21	3.34
3. He	0.150	3	16.6 ± 0.15	50.0	1.2 ± 0.2	0.60 ± 0.10	0.41	1.46
4. NH_3	0.650	3	12.0 ± 0.2	36.2	5.4 ± 0.4	2.71 ± 0.20	0.94	2.89
5. C_2H_2	0.980	1	11.0	33.2	10.7	5.37	1.19	4.51
6. Air	1.09	6	11.0 ± 0.1	33.2	7.9 ± 0.2	3.98 ± 0.09	1.32	3.02
7. O_2	1.21	2	11.45 ± 0.15	34.5	7.3	3.68	1.59	2.32
8. A	1.50	3	9.4 ± 0.03	28.3	4.1 ± 0.2	2.06 ± 0.10	1.32	1.56
9. CO_2	1.66	2	10.3 ± 0.05	31.0	11.3 ± 0.6	5.69 ± 0.30	1.76	3.23
10. C_3H_8	1.70	3	10.2 ± 0.2	30.8	12.9 ± 0.5	6.50 ± 0.25	1.77	3.67
11. Cl_2	2.70	3	9.3 ± 0.1	28.0	12.5 ± 0.3	6.28 ± 0.23	2.33	2.70

ρ_i = initial density of gas (g/cc)

V_i = velocity of ionization wave extruded into plastic tube (km/sec)

p_w = pressure in water as determined by measured shock velocity and calibration curve (kb)

p_i = pressure in incident wave as determined by the impedance mismatch equation (kb)

p_s = computed pressure of shock wave moving at the observed velocity V_p of the ionization wave in same gaseous medium ($p_i + p_1 = \rho_i V_i U_i$)

U_i = particle velocity in shock wave of velocity V_i and pressure p_i (km/sec)

M = mach number

N = number of shots

Table IV.

A. Conduction in compressed ionization waves

Gas	Ambient Pressure			0.5 mm Hg Pressure		
	R (ohm)	σ (ohm cm)$^{-1}$	L_c^* (cm)	R	σ	L_c
Argon	0.6	0.5	--	--	--	--
Air	0.6	0.5	16.5	1.2	0.25	30
Oxygen	0.6	0.5	--	--	--	--
Chlorine	1.0	0.3	--	--	--	--
Ammonia	1.9	0.16	--	--	--	--
Hydrogen	2.3	0.13	25	1.5	0.20	30
Helium	2.5	0.12	--	--	--	--
Acetylene	10.0	0.03	--	--	--	--
Propane	52.5	0.006	12	1.7	0.18	30

*L_c = length of ionization wave

B. Absolute conductivity data for compressed ionization waves from equation 2 where b = 0.416 cm, a = 0.159 cm

length (cm)	σ (ohm cm)$^{-1}$	K -measured probe factor
2.54	0.28	1. 0.23
3.81	0.39	2. 0.31
5.08	0.40	3. 0.38

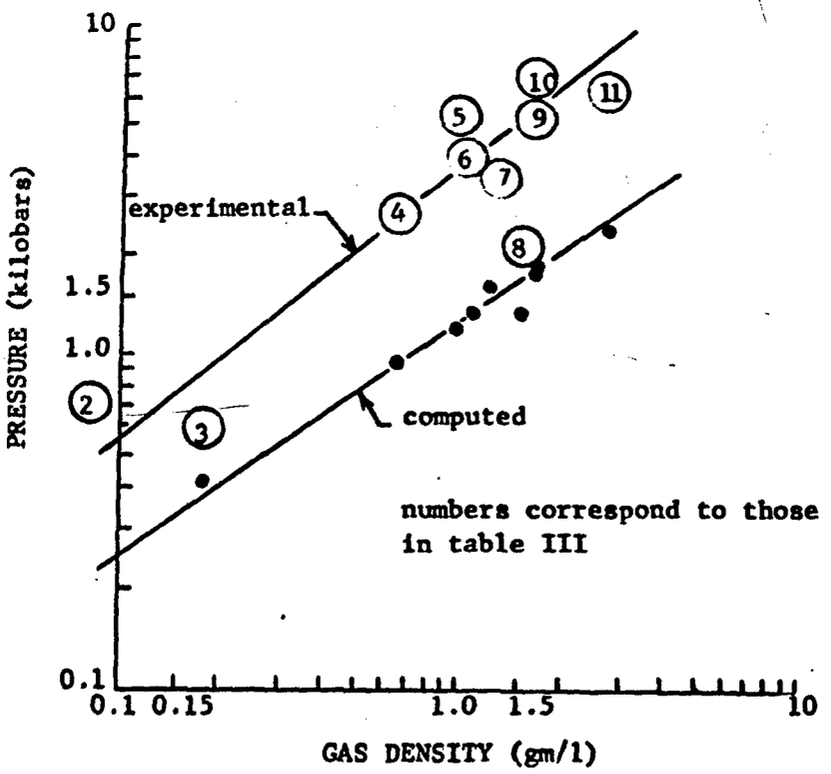

Fig. 6 Measured vs computed ionization wave (or shock) pressures as a function of density of gaseous medium.

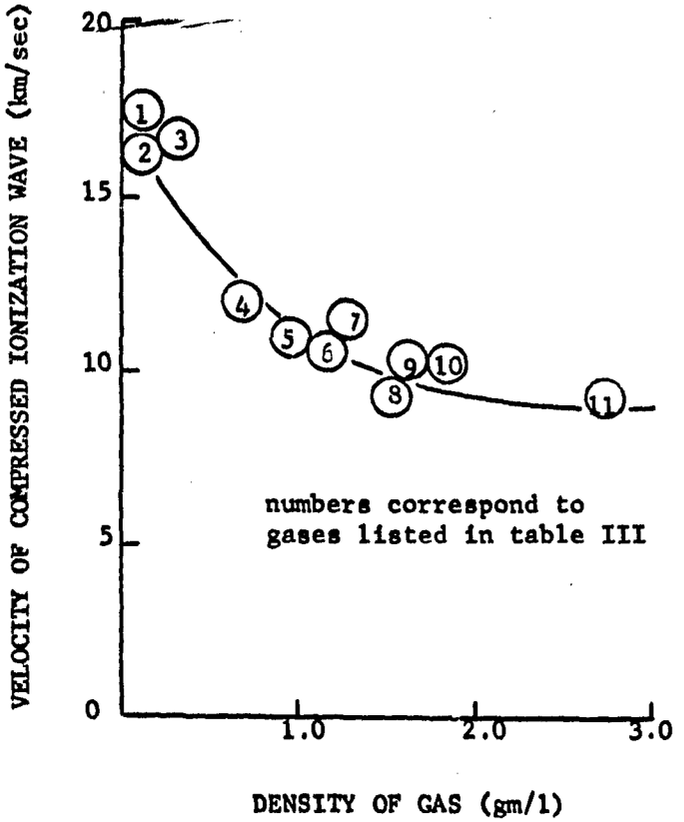

Fig. 7 Graphical correlation of data in Table I.

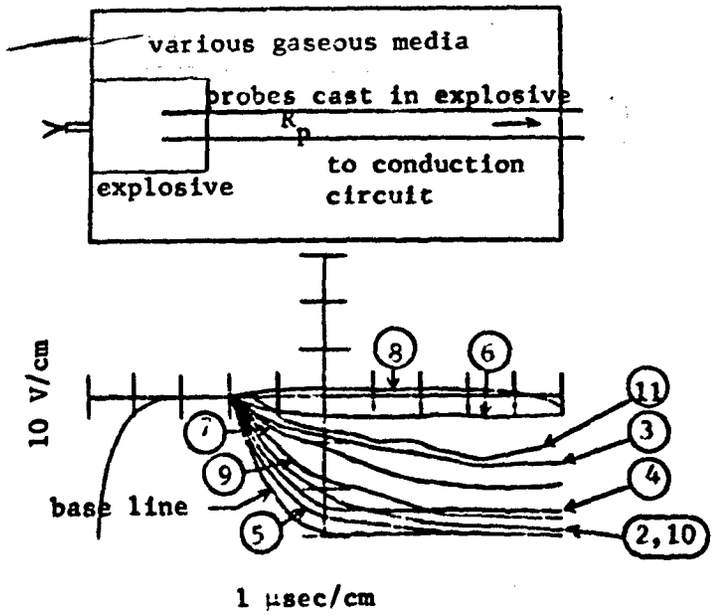

Fig. 8 Plots of oscilloscope traces of conduction in various gases as a function of time (or distance) of propagation of ionization wave from the explosive. R_l = 9 Ω, E_o = 45 volts, parallel probes ≈ 1 cm apart.

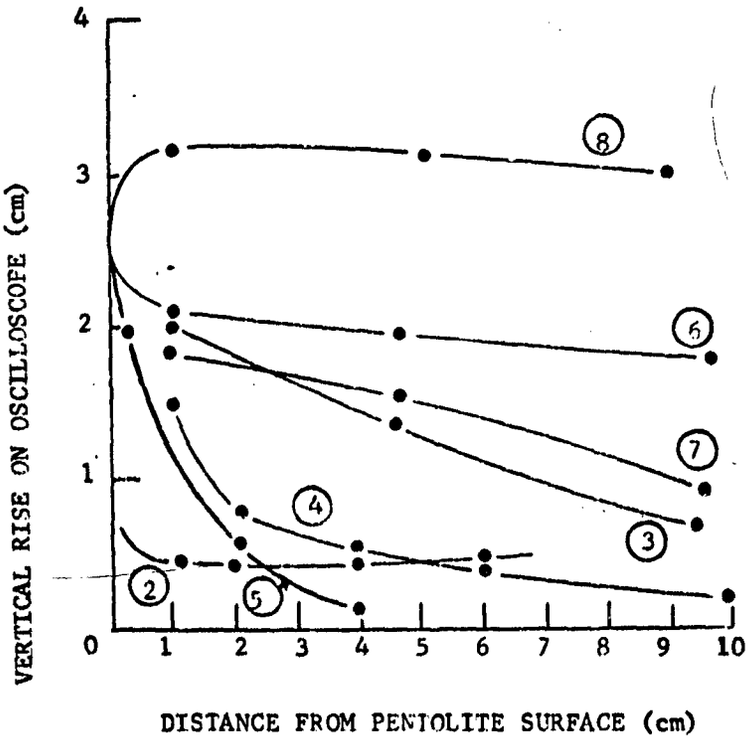

Fig. 9 Maximum conduction of freely expanding ionization waves as a function of distance from free surface of 1-1/2" X 1-1/2" D pentolite charge. Constant R_l and E_o.

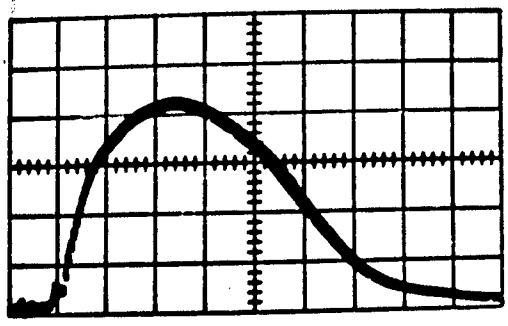

AIR 645 mm Hg.
$R_i = 2\ \Omega$

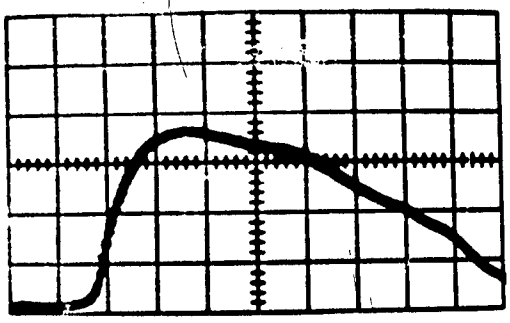

AIR 0.5 mm Hg.
$R_i = 2\ \Omega$

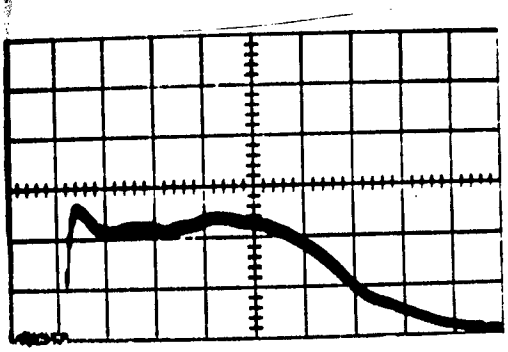

HYDROGEN 645 mm Hg.
$R_i = 10\ \Omega$

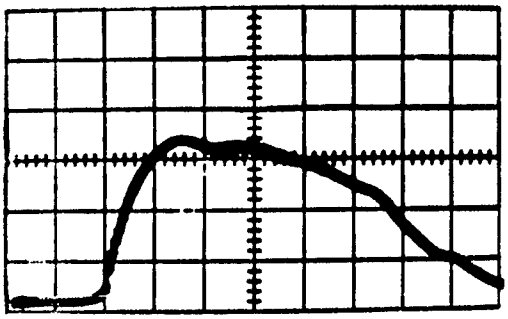

HYDROGEN 0.5 mm Hg.
$R_i = 2\ \Omega$

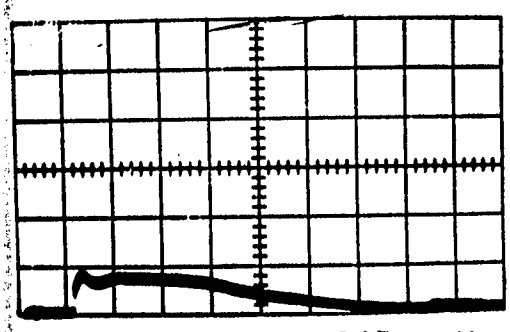

PROPANE 645 mm Hg.
$R_i = 10\ \Omega$

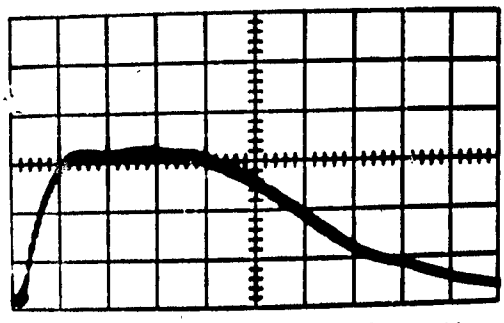

PROPANE 0.5 mm Hg.
$R_i = 2\ \Omega$

$E_0 = 25$ VOLTS
HORIZONTAL SWEEP = 2 microsec/cm
VERTICAL GAIN = 5 VOLTS/cm

Fig. 10. Typical conduction traces for ionization waves.

In comparing verticle gain, however, note that R_i was varied and the data needed to be normalized. When comparing the pulse duration it must be remembered, moreover, that the ionization traveled at a different velocity for each gas (Table III). The conduction data listed in Table IV also include data from a series of probe shots where two sets of probes were used in the plastic tube a known distance apart, and yielded an oscilloscope trace with two humps in it. This permitted comparison of the ionization wave intensity and velocity with the luminosity and velocity determined by the streak camera.

The observed conductivity data for air and hydrogen are compared with data computed from shock wave theory listed in Table V. The relative values listed permit observations and theory for air and hydrogen to be compared with the uncertain probe factor eliminated. The calculations for hydrogen were performed at this laboratory and a description is given in Appendix I. The shock theory conduction data for air were taken from Gilmore[11] and Meyer.[12] Gilmore solved the equilibrium conditions for the many species of particles in an air shock and tabulated the number of free electrons per air particle for a given initial pressure, conductivity in an air shock from the expression

$$\sigma = \frac{n_e \epsilon^2}{M_e C_e \sum n_j Q_j} \qquad (3)$$

where σ = conductivity, n_e = number density of free electrons, n_j = number density of ion species j, $\bar{Q}_j$ =Maxwell averaged total electron collision cross-section of species j, $\bar{C}_e$ = mean speed of electrons = $(8kT/\pi M)^{1/2}$, ϵ = electron charge, M_e = electron mass, k = Boltzmann constant. The only difficulty is in obtaining a value for $\bar{Q}_j$. At high temperature the positive ions become the dominant electron scattering centers by introducing a coulombic effect between the ion and electron. While the cross-section of neutral air atoms remain approximately constant ($2 \cdot 10^{-15} cm^2$) over experimental temperature ranges the ion cross sections due to coulomb

Table V:

Experimental conductivities compared with shock theory-computed conductivities

A. Air

Probe location	p_o	σ*	$\sigma_{645}/\sigma_{0.5}$	V_i	T_2	ρ_2/ρ_o	σ**	$\sigma_{645}/\sigma_{0.5}$
Near charge surface	645	0.012	0.5	8.6	13	10	29	0.2
	0.5	0.006		15	17	0.014	130	
Extruded into 3/8" plastic tube	645	0.52	2.0	11	17	10	130	0.8
	0.5	0.26		17	19	0.013	160	

B. Hydrogen

	p_o	σ*	$\sigma_{645}/\sigma_{0.5}$	V_i	T_2	σ***	$\sigma_{645}/\sigma_{0.5}$
Extruded into 3/8" tube	645	0.13	0.6	16.3	5.0	$9.25 \cdot 10^{-6}$	82
	0.5	0.20		17.0	3.3	$0.11 \cdot 10^{-6}$	

V_i = velocity of ionization wave (km/sec)

p_o = initial pressure of air (mm Hg)

T_2 = temperature in shock wave[11] ($°K \cdot 10^{-3}$)

ρ_2/ρ_o = density ratio between shock front and initial density[11].

σ = conductivity in ohms^{-1} cm^{-1}

* using experimental K from Table IV b.

** from Fig. 12

*** calculated from shock theory

interaction vary[21] from about 10^{-12} cm^2 at low temperatures (3000°) to values approaching 10^{-15} cm^2 at high temperatures (>20,000°). With assumptions of how $\bar{Q}_j$ varies with T, Meyer calculated electrical conductivities in an air shock. Figs. 11 and 12 are taken from the work of Gilmore and Meyer.

True Shock Velocity

Shock wave velocity measurements were made for shocks transmitted from Composition B through aluminum plates into air and argon. The plates were so thin the pressure drop of the shock wave in the plate was small. The velocities obtained were 4.4 km/sec for the shocks transmitted into air and 3.85 km/sec for those transmitted into argon.

Discussion of Results

Source of Luminosity and Ionization

The detonation-generated plasma concept has been criticized[6,7] on the basis that the observed luminosity is simply the result of thermal ionization and recombination in a shock wave, the difference, for example, between conductivities in air and helium presumably being caused by the greater ionization potential of helium. Luminosity, however, is not really the criterion that determines the existence or non-existence of a plasma. In a hydrogen atmosphere luminosity is also lacking even though its ionization potential (15.6) is less than that of the most brilliant luminosity generator, argon. One, of course, realizes that the shock wave pressure would be much higher in argon than in hydrogen. When Composition B is detonated in helium one does observe luminosity (Fig. 4d) over a short distance from the charge and this itself is a phenomenon that can hardly be explained by a shock mechanism. Also, although the luminosity disappears in a very short period ($\simeq$ 3μsec) the ionization continues in helium. When less powerful Dithekite-13 was used there was no visible luminosity but still strong ionization was observed. Clearly, one needs to distinguish between the ionization wave from the explosive and the ionization induced by a shock wave in a gaseous medium.

Previous electrical conduction work[4] and the data obtained here (fig. 8,9) serve to distinguish between the two sources of ionizations. In addition to the data reported here, unpublished spectroscopic studies of the ionization wave , or plasma, in argon showed carbon as well as argon in the luminous wave front. Furthermore, Funk, et al[13] showed that the luminosity of the ionization wave may be readily modified by thin films or coatings placed on the free surface of the charge, e.g., thin layers of aluminum, magnesium, lead, grease, etc.

Dithekite-13 was used for some of the present study because its products of detonation (since it is oxygen balanced) are transparent. In Fig. 4b, c, for example, the presence of detonation products in the transparent region behind the ionization wave can be detected only by a distortion of the backlight grid. Close observation of the ionization waves in hydrogen and helium reveals a diffuse, non-luminous zone at the front of the detonation products that corresponds to the luminous zone, for example, in oxygen (Fig. 4a). This fuzzy zone is not due to a shock wave alone since it is too wide to be attributed to possible camera smear effects and covers only the front part of the detonation product wave. Furthermore, with the type of diffuse backlighting used in Fig. 4, one is not able to resolve gaseous shocks of the small magnitude involved. Special techniques such as Schlieren or parallel light are needed to observe the gaseous shocks.[14] The fact that the fuzzy zone in helium is conducting is seen in Fig. 4c where the high voltage arc (approximately 20 KV) discharges as the zone reached the H.V. probe.

The low conduction (Figs. 8,9) in hydrocarbon gases, and hydrogen and ammonia, is explained on the basis of electron traps due to breaking of chemical bonds involving hydrogen atoms which soak up the free electrons. Cracking is strong in propane where the ionization wave generates a dense black cloud and its electrical conduction then becomes nil. On the other hand, as shown below, in many cases ionization of appreciable magnitude is generated by the shock wave, e.g., in argon and air.

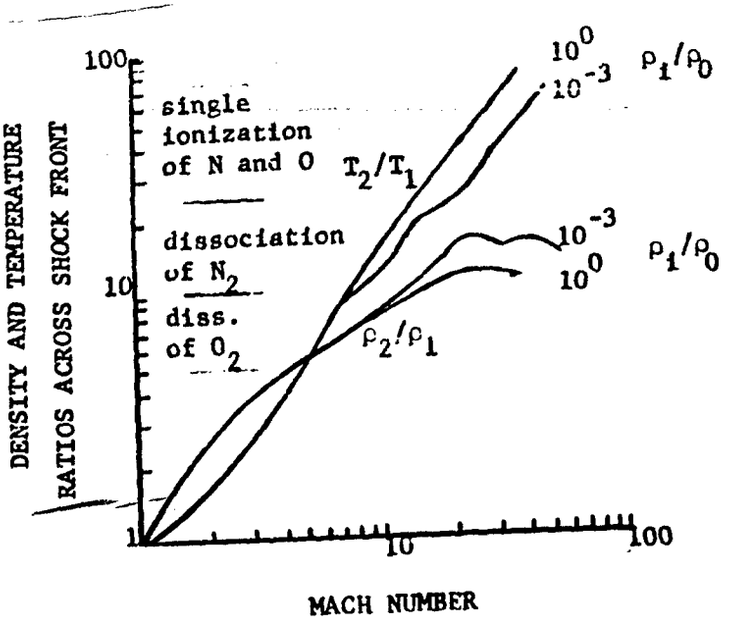

(11)

Fig. 11 Density and temperature ratios across normal shock front in air.

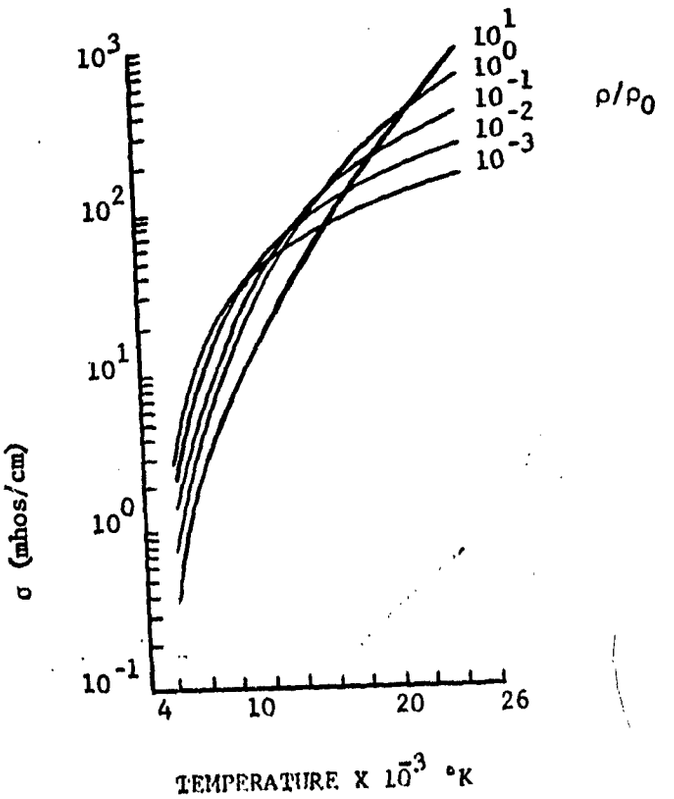

Fig. 12 Electrical conduction in an air shock wave.

Even though the ionization waves in hydrogen and helium were non-luminous they always generated high luminosity upon impacting a glass or plastic, e.g., the walls of the containers. For example, the chamber end may be seen in Figs. 4, 13 and 14 to be illuminated well ahead of the oncoming dark detonation products. For instance, in Fig. 13a the illumination occurred 2.8 μsec before the massive detonation products reached the end plate, and in Fig. 13c, involving a smaller vacuum chamber and Comp. B/AN explosive (D = 7.4 mm/μsec) the end of the chamber may be seen to have been illuminated even before the detonation reached the end of the charge. For the latter case the material causing illumination came from off the sides of the charge and reached the end of the chamber well ahead of the detonation owing to the extremely high velocity of this precusor wave. In Fig. 14 although the chamber end plate was illuminated well ahead of the detonation products impact on the plate, the pressure in the ionization wave produced no detectable shock wave (observable by this particular technique) in the plexiglas. It was several microseconds later before the cloud of detonation products impacted the plexiglas and generated the shocks seen in Fig. 14.

Shock vs Ionization Wave Pressures

The observed consistently high values of pressures in compressed ionization waves (Table III) over corresponding pressures computed for shocks traveling in the same medium at the same speed is noteworthy. By themselves, comparisions of observed vs computed pressures may not be sufficient to rule out the possibility of a shock mechanism. It may be argued, for example, that the impedance mismatch equation may not apply with sufficient accuracy.[10] On the other hand, evidence presented below shows that the actual shock wave velocity for the true shock is less than half the velocity of the ionization waves. Hence, the actual or true shock wave pressure is only about one-fourth as great as the value computed by assuming the shock wave velocity to be the same as the ionization wave. On this basis the measured ionization wave pressures were 10 to 20 times greater than the pressures in the true shock waves transmitted from the explosive into the gaseous medium.

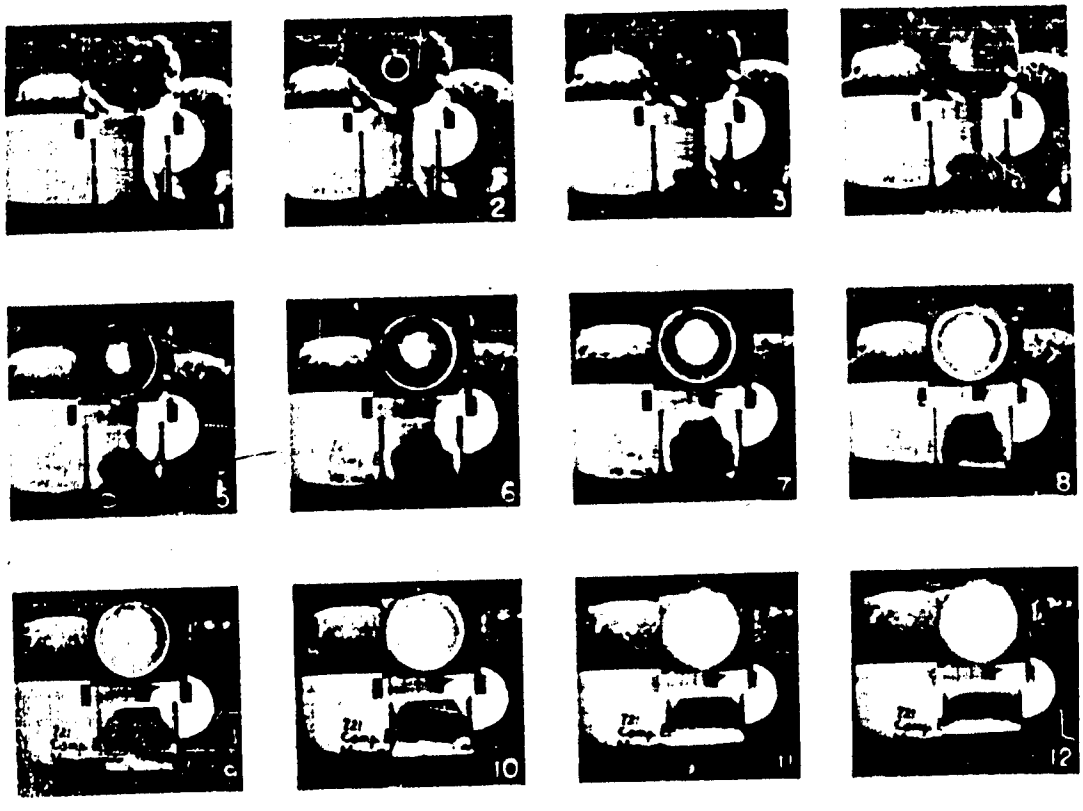

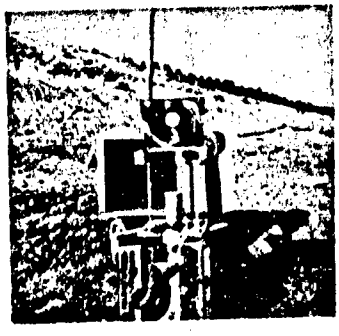

Fig. 13. Framing camera sequence and set up for vacuum shots.

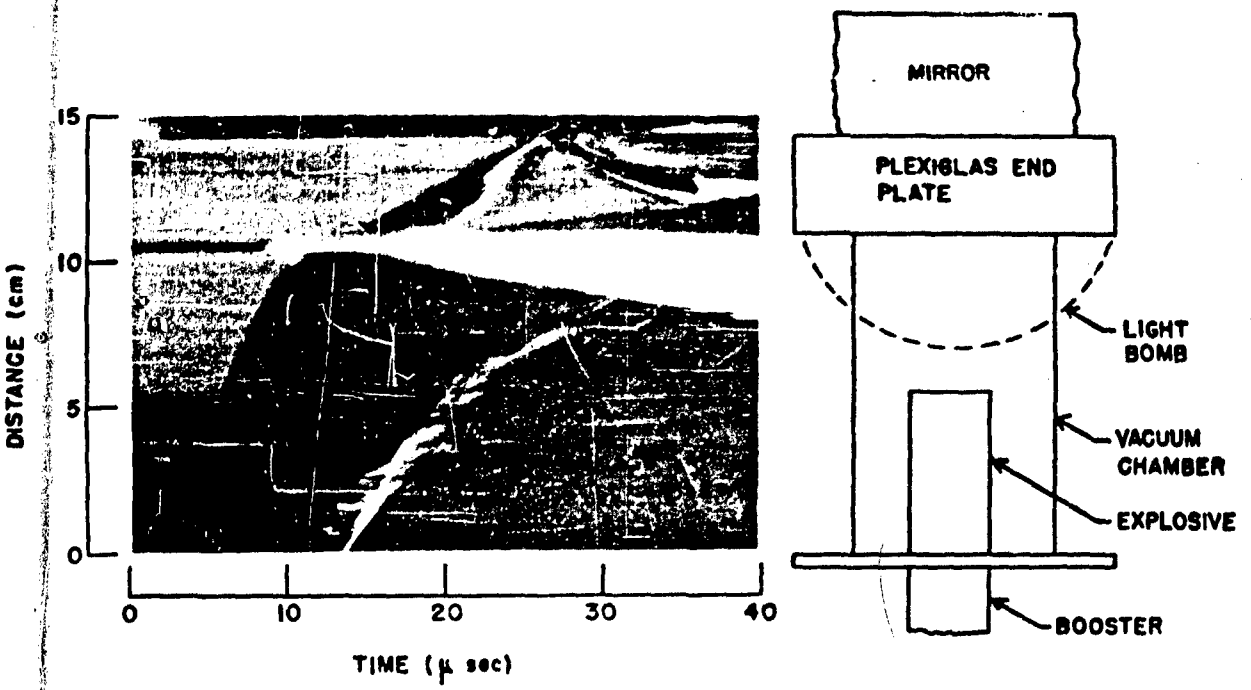

Fig. 14a. Streak camera record obtained simultaneously with the framing camera sequence in Fig. 13a.

Fig. 14b Framing camera sequence of (73/27) Comp. B/AN detonating in plastic chamber of 0.5 mm Hg Air. Inter frame time 2.08 μsec, D = 7.400 km/sec.

The conductivity data may also be criticized on several points, for example, it may be argued that surface conductivity effects between the probes[17] caused inaccurate measurements, hence an inaccurate probe factor. On the other hand, it should be noted from the results of Table IV that the conduction was almost independent of the composition of gaseous medium. Likewise, the length of the conducting zone was independent of the gaseous medium. This would be expected only if the conduction were due to ionized gaseous products from the explosive. The shape of the conduction curves is also significant in that there was a gradual rise of conduction as the ionization wave reached the probes, whereas the conduction for pure shock (Fig. 15) has a more sudden rise. The fact that conduction over the probes (in free expansion with no wall effects) increased gradually indicates that there is an increasing density of electrons leading up to the shock front.

"Precursor" Ionization Waves

It is not unexpected that electrons and perhaps low mass ions would be radiated ahead of a shock owing to its high thermal gradient. The high temperature of the shock (e.g. >10,000°K) coupled with the low ambient temperature ahead of the shock presents a tremendous driving force quite as effective as an electrical potential gradient for separating the low mass electrons from higher mass ions. Thus, it is not really surprising that electrons and the lighter ions are able to diffuse through and move ahead of the shock front. Most of the ionized material in the ionization wave definately originates (from chemiorization) on the explosive surface and is ejected into the gaseous medium when the detonation reaction zone emerges from the explosive free surface. As the surface layer of explosive is encountered by the detonation reaction some of the explosive is projected forward while it is still undergoing reaction and is thus projected into the gaseous medium before decay, promoted by high density,[4] has time to take place.

The precursor ionization wave phenomenon has been observed by Weyman[15] and by Gloersen[16] and others[22] in shock tube studies. Free electrons radiated ahead of the shock wave were detected by Weyman at more than a meter

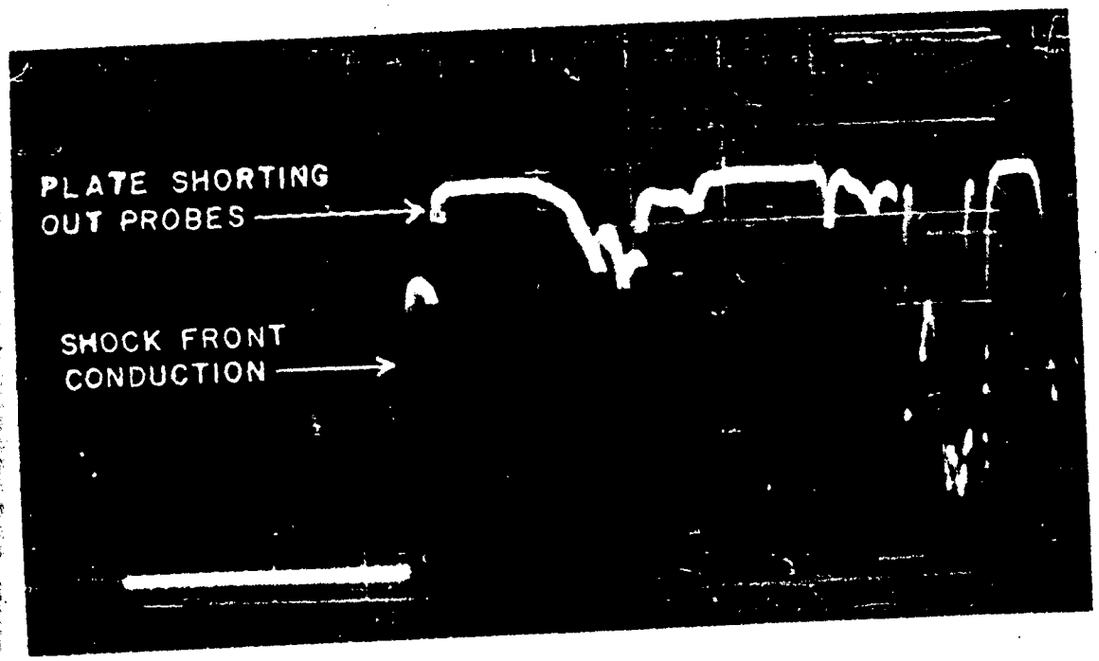

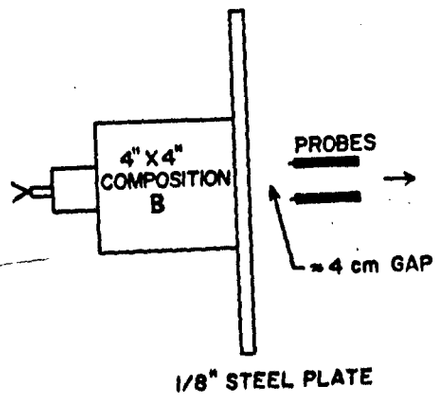

Fig. 15. Assembly and resulting conduction measurement of shock in air driven by steel plate.

in front of the shock wave and the General Telephone and Electronics Laboratories [22] determined electron density of 10^{11} to 10^{13} electrons/cc build up over a distance of approximately 15 cm in front of the shock wave in a shock tube.

Velocity of Shock Generated by High Explosives in Gaseous Media

The more general assumption is that the brilliantly luminous ionization waves from high explosives are simply intense air shock waves in which ionization arises by thermal means. It has generally been overlooked that the observed velocities would imply a breakdown of the hydrodynamic theory of transmission of shock waves. That is, if the ionization waves were truly shock waves one might well wonder by what mechanism they acquire such high velocities and pressures, i.e. why the waves radiated from free surfaces of high explosives have velocities about twice as great as waves of the same or higher intensity transmitted from inert, e.g., metal, surfaces into air. For example, the velocity of the observed luminous wave transmitted from Composition B directly into air at atmospheric pressure was 8.3 km/sec, but when an aluminum plate thin enough so that there was no appreciable attenuation of the wave, as determined by actual pressure measurements by the aquarium method [8,9], was placed on the end of the charge the shock wave was observed at only 4.4 km/sec. For argon corresponding velocities were 8.57 and 3.85 km/sec. respectively.

Careful examination of the application of the impedance mismatch equation (1) has been made for shock wave transmitted from Composition B into five solids and five liquids of widely different densities. For the liquids Fig. 16 presents the measured velocity-pressure curves obtained by the aquarium method. Table VI presents the observed initial shock velocities and pressures computed from the impedance mismatch equation. The consistency is excellent and the results are in close agreement with those of the Los Alamos group [18,20] showing that the impedance mismatch equation applies very well to liquids and solids.

As another check on consistency U_i/V_i values were compared with $(v_i-v)/v_i$ results computed from the Tait equation of state and the theoretical equation of state derived by Cook. [19] Table VI presents parameters used in these computations. Note the excellent agreement between the observed U_i/V_i

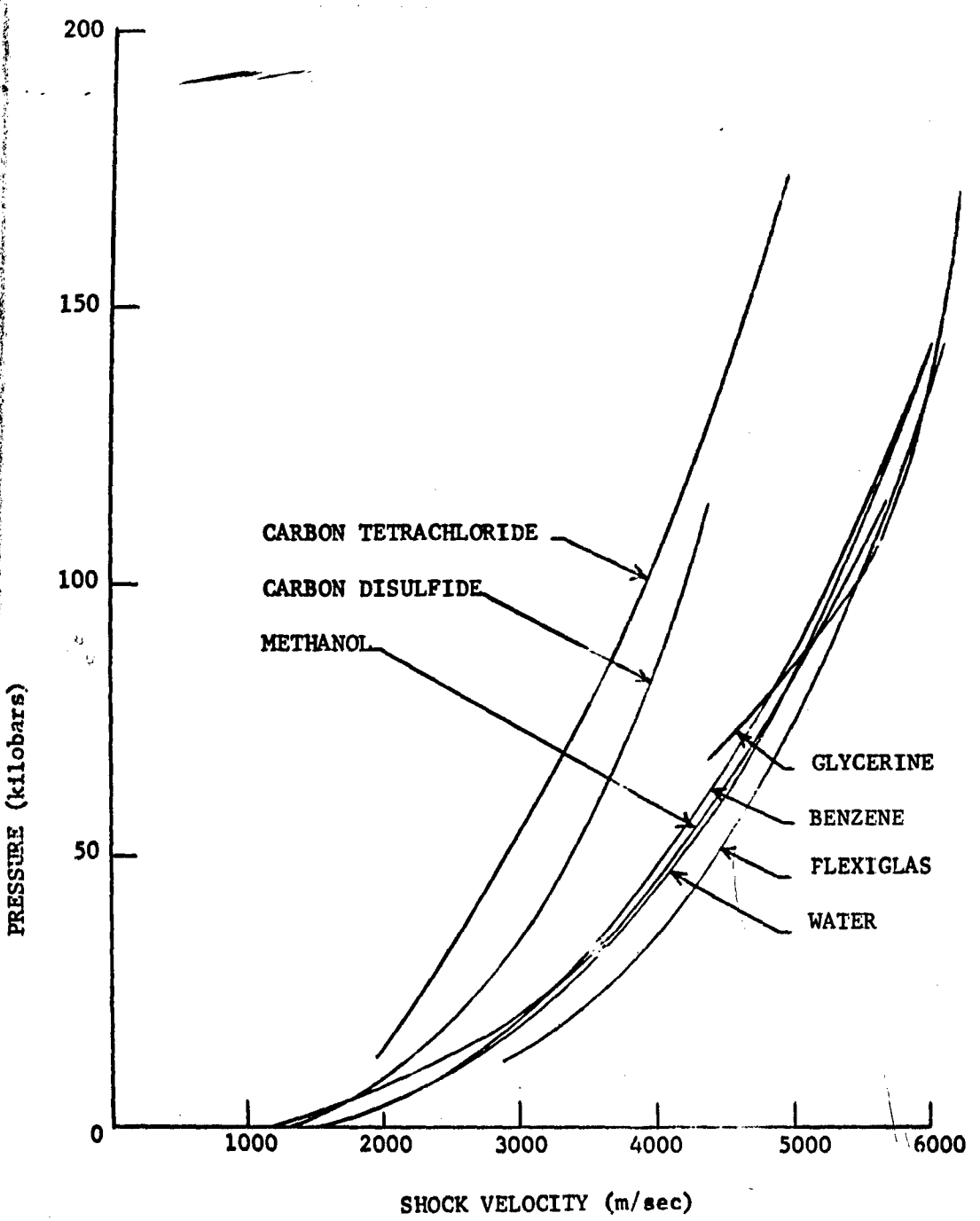

Fig. 16 Experimental velocity vs pressure curves for shocks in various liquids.

Table VI: Initial properties of shock waves transmitted from Composition B ($\rho_1 D$ = 13.4 kmg/sec cc) into various media.

Medium	ρ_i g/cc	β_o^{-1} ($atm^{-1} \cdot 10^4$)	C	V_i obs. km/sec	U_i^+ km/sec	p_i^+ kb	V_p km/sec	p* kb	$p^\ddagger$ kb	U_i/V_i	$(v_i - v)/v_i$
H_2	$7.0 \cdot 10^{-5}$	--	--				10.4	~0.01	0.065		
He	$1.4 \cdot 10^{-4}$	--	--	3.10++	2.83++		8.7	~0.02	0.09	0.915	
Air	10^{-3}	--	--	4.44	3.98	0.18	8.3	0.15	0.62	0.898	0.896
Argon	$1.4 \cdot 10^{-3}$	--	--	3.85	2.85	0.15	8.6	0.18	0.90	0.740	
Methanol	0.8	1.22	(0.13)	5.50	2.50	--	--	110	--	0.455	0.455**
Benzene	0.88	0.97	(0.13)	5.60	2.54	--	--	125	--	0.454	0.455
Water	1.00	0.46	0.1365	5.88	2.39	--	--	140	--	0.409	0.409
CCl_4	1.60	1.67	0.0925	4.85	2.27	--	--	172	--	0.469	0.469
Mercury	13.55	0.0367	0.12	3.61	0.81	--	--	350	--	0.255	0.255
Magnesium	1.735	0.295	0.5	6.70	3.20	--	--	215	--	0.48	0.44***
Beryllium	1.85	0.0855	0.5	9.60	1.52	--	--	265	--	0.16	0.17
Aluminum	2.70	0.134	0.5	7.24	1.38	--	--	280	--	0.19	0.24
Iron	7.86	0.0587	0.5	5.18	0.88	--	--	355	--	0.17	0.16
Copper	8.90	0.0719	0.5	5.11	0.77	--	--	325	--	0.15	0.17

‡ Computed assuming ionization wave to be a shock wave
+ Computed from known p-V-T data and the observed velocity V_i
* From impedance mismatch equation
** From Tait equation and p*
*** Computed from $(v_o - v)/v_o = 1 - (1 + 2\,\beta_o p)^{-1/2}$
V_i = velocity of shocks for gases measured for thin Al plates
++ Measurements taken thru Al plate
Tait equation: $\beta = C/(L + p)$; $L = C\beta_o$ (from Cook's equation of state)

and computed $(v_i - v)/v_i$ results. (Note that from hydrodynamic theory $U_i/V_i = (v_i - v)/v_i$.) Considering such wide differences in shock impedance as, for example, between Composition B into methanol as compared with Composition B into mercury, magnesium, and copper, the impedance mismatch equation thus seems to have quite general applicability. Even more significant is the fact that it applies quite accurately in predicting the shock velocity (or pressure) of a shock transmitted ~~into~~ air and argon through a thin metal, e.g., an aluminum plate, as shown in Table VI. These considerations therefore provide strong evidence that the ionization waves from free surfaces of high explosives are not true shock waves because their velocity characteristics are quite different from those computed from the well-established shock wave theory and the impedance mismatch equation.

Conclusions

1. Luminosity is observed when detonation plasmas propagate through many gaseous media, but luminosity is not the determining criteria of plasma existence. The luminosity is caused by interaction of electrons in the plasma with molecules of the gaseous medium (largely via negative ion formation). If negative ions are not obtained, i.e., if there is no electron affinity, as in helium, no medium (vacuum), or if there is rapid ionization decay due to free radicals, there may be no visible, or only a transient luminosity associated with the plasma even though it initially may be rich in free electrons.

2. The measured pressures of (compressed) plasma are consistently up to five times higher than corresponding shock pressure of the same velocity.

3. Absolute conductivity measurements in air show insufficient differences relative to those computed for the shock wave theory, and are not conclusive in themselves. However, the situation is quite different for hydrogen, helium, and other gases where shock wave theory can in no way account for the high observed conductivities. The shapes of the conduction traces are quite different than for shock waves, but agree more with the

concept of detonation-generated plasmas associated with, but sieving ahead of the shock wave.

4. The precursor ionization wave or plasma is generated primarily from chemionization in the detonation reaction zone and is ejected into and trapped in the low density state of the shock upon reaching the free surface of the explosive. The ionized surface material is then propagated ahead of the normal shock where it interacts with the gaseous medium to produce high luminosity in many cases.

5. The velocity of the ionization waves radiated from free surfaces of high explosives are much greater than can be accounted for by classical hydrodynamic theory of shocks and is likewise much higher than one observes for shocks transmitted into gaseous media from inert solid free surfaces.

BIBLIOGRAPHY

1. Cook, M.A., The Science of High Explosives, Reinhold Publishing Corp., N.Y.(1958).
2. Cook, M.A., McEwan, W.S., J. Appl. Phys. 29, 1612 (1958).
3. Cook, M.A., Pack, D.H., and Gey, W.A., Seventh International Symposium on Combustion, London, September 1958.
4. Cook, M.A., Keyes, R.T., and Udy, L.L., J. Appl. Phys., 30, 1881 (1959).
5. Bauer, A., Cook, M.A., and Keyes, R.T., Proc. Roy. Soc., A259, 508 (1961).
6. Davis, W.C., and Campbell, A.W., J. Appl. Phys., 31, 1225, (1960).
7. Kendrew, E.L., and Whitbread, E.G., 3rd ONR Symposium on Detonation, Princeton University, 1960.
8. Cook, M.A., Pack, D.H., and McEwan, W.S., Trans. Fara. Soc., 56, 1028 (1960).
9. Cook, M.A., and Udy, L.L., J. Am. Rocket Soc., 31 52 (1961).
10. Walsh, J.M., and Christian, R.H., Phys. Rev. 97, 1955 (1955).
11. Gilmore, F.R., Rand Research Memorandum RM 1543, August 1955.
12. Meyer, R.X., J. Am. Rocket Soc., 29, 187 (1959).
13. Cook, M.A., Funk, A.G., Keyes, R.T., 3rd ONR Symposium on Detonation, Princeton University, 1960.
14. Deal, W.E., Jr., J. Appl. Phys., 28 782 (1957).
15. Weymann, A.D., Physics of Fluids, 3, 545 (1960).
16. Gloersen, P., Physics of Fluids, 3,857 (1960).
17. Lin, S.C., Resler, E.L., and Kantrowitz, A., J. Appl Phys., 26, 95 (1955).
18. Deal, W.E., Jr., Second ONR Symposium on Detonation, Washington, D.C., February 9-11, 1955.
19. Cook, M.A., Fara. Soc. Disc., No. 22, 203 (1956);Bulletin #74, 46, No. 16, November 1955 (Utah Engineering Experiment Station, Univ, of Utah); J. Appl. Phys., 30, 729 (1959).
20. Walsh, J.M., and Rice, M.H., J. Chem. Phys., 26, 818 (1953)
21. Bachynski, M.P., Shkarofsky, I.P., Johnston, T.W., R.C.A. Research Laboratory, Research Report No 7-801.3 (June 1959).
22. General Telephone & Electronics Laboratories Inc. Palo Alto, California., "Energy Transfer in Plasmas", Technical note no. 7, 15 November 1960.

APPENDIX I: THEORETICAL RESULTS FOR SHOCK WAVES IN HYDROGEN

The first step was the calculation of the dissociation products in the shock wave corresponding to a given initial specific volume (v), a given compression ratio (v_o/v), and an assumed shock temperature (T_2). The species considered were H_2, H, H_2^+, H^- and ϵ^-. The method used follows that of Cook,[1] the appropriate chemical equilibria being expressed as follows:

$$H \leftrightarrows 1/2H_2 \qquad K_3 = \frac{(H)}{(H_2)^{1/2}} F^{1/2} \qquad (1)$$

$$H_2 \leftrightarrows H_2^+ + \epsilon^- \qquad K_{30} = \frac{(H_2)}{(H_2^+)\ (\epsilon^-)} F^{-1} \qquad (2)$$

$$H \leftrightarrows H^+ + \epsilon^- \qquad K_{31} = \frac{(H)}{(H^+)\ (\epsilon^-)} F^{-1} \qquad (3)$$

$$H^- \leftrightarrows H + \epsilon^- \qquad K_{32} = \frac{(H^-)}{(H)\ (\epsilon^-)} F^{-1} \qquad (4)$$

where a ( ) signifies the concentration of the enclosed species in gram atoms per 100g of the initial mixture, hydrogen. The symbol, F, denotes the fugacity factor, which (since the ideal gas equation applies in this case) has the value

$$F = 1/v \qquad (5)$$

The values for K_3 as a function of temperature are listed in reference (1). The remaining K's were calculated from Saha's equation expressed in the form

$$\log K_p = (-5024\ I_a)/T + 5/2 \log T + \log (g_i g_\epsilon / g_a) - 6.47 \qquad (6)$$

where I_a is the ionization potential in electron volts and g_i, g_ϵ, and g_a are the statistical weights of the ion, the electron, and the atom, respectively, with the exception of reaction (4) where g_i was the statistical weight of the atom and g_a was the statistical weight of the negative ion. The values of I_a used for reactions 2,3 and 4 where respectively 15.6, 13.53 and 0.75. The K_1's of equations 2,3 and 4, which are defined in terms of the concentrations

of the species, are related to the partial pressure K_p's of equation (6) by the expression

$$K_i = K_{p_i}^{-1} (1.2181/T)^{-1} \qquad (7)$$

Equations 1,2,3 and 4 may each be expressed in terms of two independent variables. The variables chosen were (H_2) and (ϵ^-), the result being

$$(H) = \gamma_3 (H_2)^{1/2} \qquad \gamma_3 = K_3 F^{-1/2} \qquad (8)$$

$$(H_2^+) = \frac{\gamma_{30}(H_2)}{(\epsilon^-)} \qquad \gamma_{30} = \frac{1}{K_{30} F} \qquad (9)$$

$$(H^+) = \frac{\gamma_{31} (H_2)^{1/2}}{(\epsilon^-)} \qquad \gamma_{31} = \frac{K_3 F^{-3/2}}{K_{31}} \qquad (10)$$

$$(H^-) = \gamma_{32} (H_2)^{1/2} (\epsilon^-) \qquad \gamma_{32} = K_{32} K_3 F^{1/2} \qquad (11)$$

The series of relations 8,9, 10, 11 together with the mass balance equations

$$2H_2 + H + H^- + H + 2H_2^+ = H_o \qquad (12)$$

$$H_2^+ + H^+ - H^- = \epsilon^- \qquad (13)$$

are sufficient to define the species for each given set of conditions (H_o is the number of gram atoms of hydrogen per hundred grams of gas). These equations, being non-linear, were solved by iterative methods. The procedure was facilitated, however, by the fact that by combining equations 9,10,11 and 13, (ϵ^-) can be related to (H_2) as follows:

$$(\epsilon^-)^2 = \frac{\gamma_{30}(H_2) + \gamma_{31} (H_2)^{1/2}}{1 - \gamma_{32} (H_2)^{1/2}} \qquad (14)$$

Thus, for the desired specific volume v_o one would,

(1) select the compression ratio v_o/v for which the shock conditions were desired, v being the specific volume under shock conditions. The corresponding fugacity factor was then calculated from equation (5).

(2) A guess was then made of the shock temperature T_2 corresponding to the chosen initial specific volume and the compression ratio.

(3) The equilibrium constants were calculated from equations 6 and 7 and the γ's from equations 8,9, 10 and 11.

(4) A value for (H_2) was next selected and the corresponding (ϵ^-) calculated from equation (14).

(5) Through use of equations 8,9, 10 and 11 (H), (H_2), (H^+) and (H^-) were calculated.

(6) These values were substituted into the mass balance equation (12), the solution being correct when this equation was satisfied, the value of (H_2) being adjusted to facilitate this.

(7) The quantities n, Q and $\bar{C}_v$ where n is the number of moles of gas at shock conditions, Q is the chemical heat, and $\bar{C}_v$ is the average heat capacity between the initial and the final temperature were calculated per kilogram of gas by the equations

$$\begin{aligned} n &= 10\Sigma_i n_i \\ Q &= 10\Sigma_i n_i Q_i \\ \bar{C}_v &= 10\Sigma_i n_i \bar{C}_{v_i} \end{aligned} \tag{15}$$

The thermochemical solution must be consistent with hydrodynamics. This occurs when the "guessed" value of the shock temperature equals the value that actually corresponds to the initial specific volume and the compression ratio selected. The shock temperature is given by the relation

$$T_2 = T_1 + \frac{1/2(p + p_o)(v_o - v) + Q}{\bar{C}_v} \tag{16}$$

where T_1 is the temperature of the unshocked gas, $1/2(p + p_o)(v_o - v)$ is the Hugoniot compressional energy and Q is the energy of chemical reactions in the shock wave. By means of the ideal gas equation of state which is applicable to the high temperature, relatively low pressure conditions of interest the shock pressure was calculated using the "guessed" value of the

temperature, the chosen specific volume under the shocked conditions, and the number of moles of gas from the thermochemical calculations, namely

$$p = nRT_2/v \qquad (17)$$

With this computed value of the pressure the shock temperature could then be calculated from equation 16 using the $\bar{C}_v$ and Q determined from the thermochemical calculations (step 5 above). If the resulting T_2 was the same as the "guessed" T_2, a self consistent solution had been obtained. Otherwise, a new temperature was selected and the whole process was repeated until agreement was achieved. In order to facilitate the rapid convergence of the temperature it was helpful to plot the "guessed" T's vs the resulting T's calculated from equation (16) as shown in Fig. a.

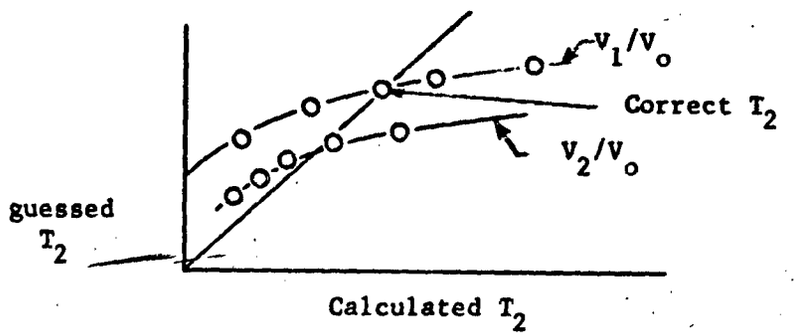

Fig. a "guessed" vs calculated T's

For hydrogen there were two solutions for some compression ratios; the correct solution being the one in which the temperature varied correctly with the compression ratio. The velocity of the shock wave was then obtained from the well know equation

$$V = v_o \frac{(p - p_o)^{1/2}}{(v_o - v)} \qquad (18$$

and the particle velocity from

$$U = \frac{p - p_o}{\rho_o V} \qquad (19)$$

The above process was carried out for a sufficient number of different compression ratios and the same initial specific volume that fairly accurate plots of the results could be made. The electrical conductivities were then calculated by the methods of Meyer.[12]

The results of the calculations are shown graphically in Fig. b and tabulated results in Table i. In addition to the calculations for the specific volume approximately equal to atmospheric pressure one calculation was made for initial conditions corresponding to 10^{-3} atmospheres in order to compare with experimental data on conduction in the hydrogen at this pressure. The comparison of experimental conduction and calculated theoretical conduction is seen in Table V (in body of the report).

Fig. b Compression ratio, temperature and electron density as functions of shock velocity in hydrogen $v_1 = 11.12 \times 10^3$ cm3/gm

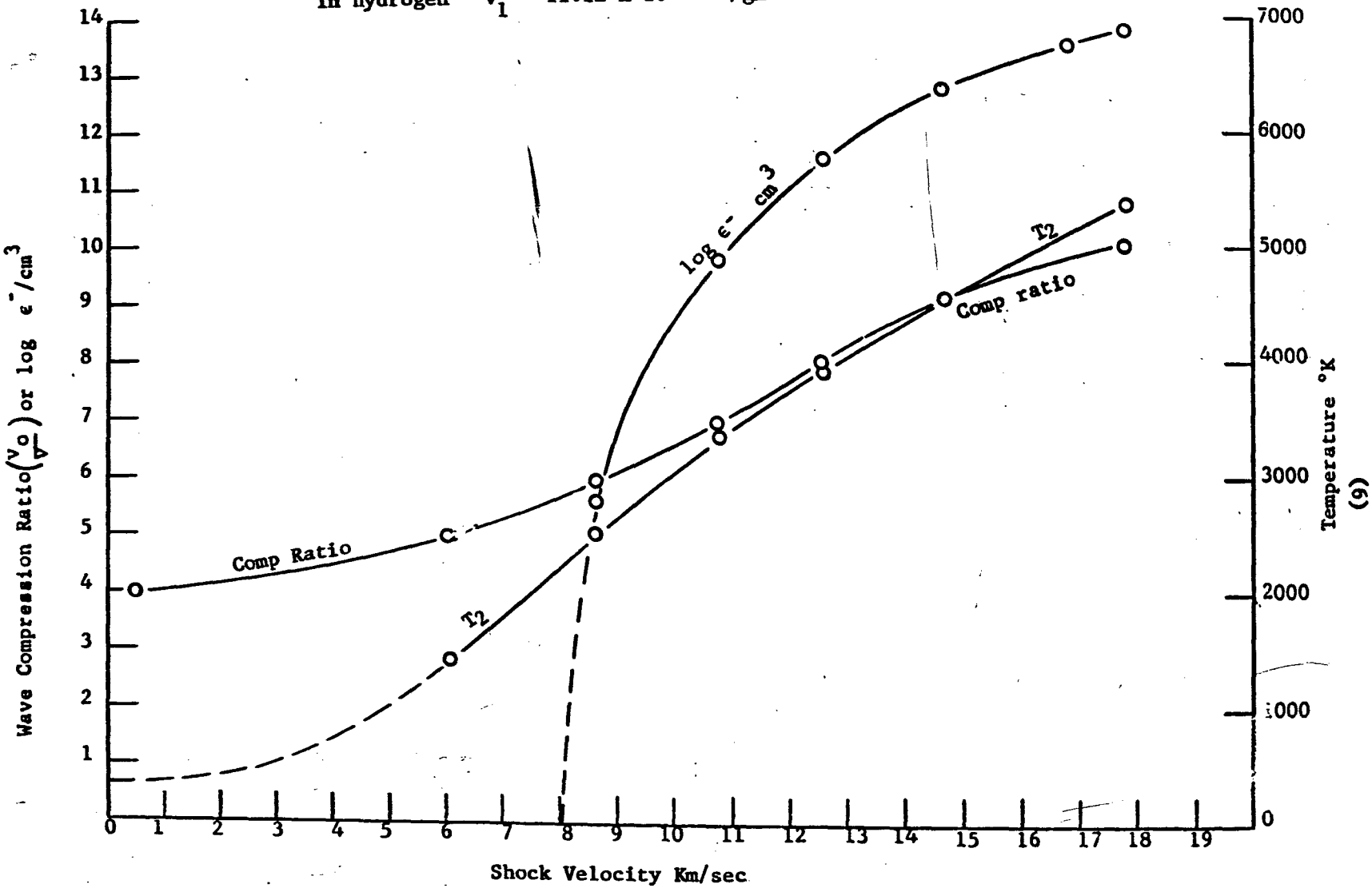

TABLE i. Calculated Characteristics of a Shock Wave in Hydrogen

A. $v_o = 11.12 \times 10^3$ cm^3/gm

$\frac{v_o}{v}$	P_2 atm.	T_2 °K	V Km/sec	ϵ^-/cm^3	Concentration of species (moles/100 gms gas) H_2	H	H_2^+	H^+	H^-	ϵ^-
5:1	26.94	1450	6.045	2.37 (-6)	50.39	1.023 (-4)	1.01 (-26)	7.75 (-26)	7.03 (-28)	8.76 (-25)
6:1	55.20	2510	8.63	4.10 (5)						1.26 (-13)
7:1	89.15	3350	10.77	5.40 (9)	49.22	2.350	8.71 (-11)	1.34 (-9)	2.82 (-8)	1.15 (-9)
8:1	123.5	3950	12.55	2.90 (11)						6.68 (-8)
9:1	169.7	4525	14.62	5.66 (12)	42.71	13.78	1.09 (-7)	1.75 (-6)	7.01 (-7)	1.16 (-6)
10:1	252.6	5380	17.74	4.78 (13)	30.46	28.27	7.87 (-6)	1.20 (-14)	6.90 (-6)	8.83 (-6)

B. $v_o = 11.12 \times 10^6$ cm^3/gm

14:1	0.240	3340	17.06	7.0 (8)						9.25 (-8)

Note
2 (-6) indicate exponent (i.e. 2×10^{-6})

DISTRIBUTION LIST

	No. of copies
Commander AF Office of Scientific Research ATTN: SRY Washington 25, D.C.	3
Commander AF Research Division ATTN: RRRTL Washington 25, D.C.	2
Commander Wright Air Development Division ATTN: WWAD Wright-Patterson Air Force Base Ohio	4
Commander AF Cambridge Research Laboratories ATTN: CRREL L. G. Hanscom Field Bedford, Massachusetts	1
Commander Rome Air Development Center ATTN: RCOIL-2 Griffiss Air Force Base Rome, New York	1
Commander Detachment 1 Hq AF Research Division The Shell Building Brussels, Belgium	2
P. O. Box AA Wright-Patterson Air Force Base Ohio	1
Aeronautical Research Laboratories ATTN: Technical library Building 450 Wright Patterson Air Force Base Ohio	1
Director, Department of Commerce Office of Technical Services Washington 25, D.C.	1
Armed Services Technical Info. Agency ATTN: TIPCR Arlington Hall Station Arlington 12, Virginia	10
Director of Research and Development Headquarters, USAF ATTN: AFDRD Washington 25, D.C.	1
Office of Naval Research Department of the Navy ATTN: Code 420 Washington 25, D.C.	1
Director, Naval Research Laboratory ATTN: Technical Information Officer Washington 25, D.C.	1
Director, Army Research Office ATTN: Scientific Information Branch Department of the Army Washington 25, D.C.	1
Chief, Physics Branch Division of Research U. S. Atomic Energy Commission Washington 25, D.C.	1
U. S. Atomic Energy Commission Technical information Extension P. O. Box 62 Oak Ridge, Tennessee	1
National Bureau of Standards Library Room 203, Northwest Building Washington 25, D.C.	1
Physics Program National Science Foundation Washington 25, D.C.	1
Director, Office of Ordnance Research Box CM, Duke Station Durham, North Carolina	1

ARO, Inc.
ATTN: AEDC Library
Arnold Air Force Station
Tullahoma, Tennessee 1

Commander
AF Flight Test Center
ATTN: FTOTI.
Edwards Air Force Base
California 1

Commander
AF Special Weapons Center
ATTN: SWOI
Kirtland Air Force Base
New Mexico 1

Commander
AF Missile Development Center
ATTN: HDOI
Holloman Air Force Base
New Mexico 1

Commander
Army Rocket & Guided Missile Agency
ATTN: ORDXR-OTL
Redstone Arsenal
Alabama 1

Commandant
Air Force Institute of Technology
(AU) Library
MCLI-LIB, Bldg. 125, Area A
Wright-Patterson Air Force Base
Ohio 1

Commander
Air Research and Development Command
ATTN: RDR 2
RDRA 1
RDRB 1
RDRC 1
RDRS 1
Andrews Air Force Base
Washington 25, D.C.

Rand Corporation
1700 Main Street
Santa Monica, California 1

Commanding General
U.S. Army Signal Corps Research
and Development Laboratory
ATTN: SIGFM/EL-RPO
Ft. Monmouth, New Jersey 1

National Aeronautics & Space
Administration
Washington 25, D.C. 6

Advanced Research Projects Agency
Washington 25, D.C. 1

Chairman
Canadian Joint Staff
for DRB/DSIS
2450 Massachusetts Ave., N.Y.
Washington 25, D.C. 1

Commander
Air Proving Ground
Attn: ACOT
Eglin Air Force Base
Florida 1

Commander
Wright Air Development Center
ATTN: WCRTM-1
Wright-Patterson Air Force Base
Ohio 1

Director, Office of Naval Research
Chicago Branch Office
86 East Randolph Street
Chicago 1, Illinois 1

Commanding Officer
Aberdeen Proving Ground
ATTN: Terminal Ballistic Lab. 1
WSL 1
Aberdeen, Maryland

Institute for Air Weapons Research
Museum of Science and Industry
University of Chicago
Chicago 37, Illinois 1

Armour Research Foundation
33 West 33rd Street
Illinois Institute of Technology
Chicago, Illinois 1

Commanding Officer
Frankford Arsenal
Attn: Director, Pitman-Dunn Lab
Philadelphia 37, Pennsylvania 1

Commanding Officer
Picatinny Arsenal
Attn: Technical Division
Dover, New Jersey 1

Chief, Bureau of Naval Weapons
Research and Development Division
Department of the Navy
Washington 25, D.C. 1

Commanding Officer
U. S. Naval Ordnance Test Station
ATTN: Technical Library
Inyokern, China Lake, California 2

Dr. P. Whitman
Applied Physics Laboratory
Johns Hopkins University
Silver Spring, Maryland 1

Mr. H. W. Wells
Carnegie Institution of Washington
Department of Terrestrial Magnetism
5241 Broad Branch Road, N.W.
Washington 15, D.C. 1

Stanford Research Institute
Poulter Laboratories Document Custodian
Menlo Park, California 1

U. S. Department of the Interior
Bureau of Mines
4800 Forbes Avenue
Pittsburgh 13, Pennsylvania
ATTN: M.P. Benoy, Reports Librarian
Division of Explosives
Technology 1

Applied Mechanics Reviews
South West Research Institute
8500 Culebra Road
San Antonio 6, Texas 1

National Bureau of Standards
Plastics Section
Attn: Dr. Olive Engel
Washington 25, D.C. 1

National Bureau of Standards
Boulder Laboratories
Boulder, Colorado 1

Dr. E. Paul Palmer
Ramo-Wooldridge Corporation
Guided Missile Division
P. O. Box 45564
Air Port Station
Los Angeles 45, California 1

Commander
U. S. Naval Proving Ground
ATTN: Warhead and Terminal Ballistics
Lab., Research Division
Dahlgren, Virginia 1

Institute of the Aeronautical Sciences
ATTN: Librarian
2 East 64th Street
New York 16, N.Y. 1

Colorado School of Mines
ATTN: J. S. Rinehart
Golden, Colorado 1

Commanding Officer
U. S. Naval Propellant Plant
ATTN: Technical Library
Indian Head, Maryland 1